REPORT DOCUMENTATION PAGE

Form Approved
OMB No. 0704-0188

1. REPORT DATE (DD-MM-YYYY)	2. REPORT TYPE	3. DATES COVERED (From - To)
21-01-2008	Final	01/06/2006 – 31/05/2007

4. TITLE AND SUBTITLE
UNDERSTANDING MICRO-RAMP CONTROL FOR SHOCK BOUNDARY LAYER INTERACTIONS

5a. CONTRACT NUMBER
FA9550-06-1-0387

5b. GRANT NUMBER

5c. PROGRAM ELEMENT NUMBER

6. AUTHOR(S)
HOLGER BABINSKY

5d. PROJECT NUMBER

5e. TASK NUMBER

5f. WORK UNIT NUMBER

7. PERFORMING ORGANIZATION NAME(S) AND ADDRESS(ES)

CAMBRIDGE UNIVERSITY
TECHNICAL SERVICES LTD
10 TRUMPINGTON STREET
CAMBRIDGE CB2 1QA
UNITED KINGDOM

8. PERFORMING ORGANIZATION REPORT NUMBER

9. SPONSORING / MONITORING AGENCY NAME(S) AND ADDRESS(ES)
USAF, AFRL
AF OFFICE OF SCIENTIFIC
875 N. RANDOLPH ST. ROOM 3112
ARLINGTON VA 22203

AFRL/VAAI

Dr John Schmisseur /NA

10. SPONSOR/MONITOR'S ACRONYM(S)

11. SPONSOR/MONITOR'S REPORT NUMBER(S)

12. DISTRIBUTION / AVAILABILITY STATEMENT

Approved for public release,
distribution unlimited

AFRL-SR-AR-TR-08-0074

13. SUPPLEMENTARY NOTES

14. ABSTRACT

This research investigated the potential of micro-ramp sub-boundary layer vortex generators for flow control of oblique shock boundary layer interactions (SBLIs) which is relevant to supersonic engine inlets. These novel devices can delay shock-induced separation and improve boundary layer health, thus offering the potential to reduce the bleed requirement in intakes. Micro-ramp Experiments have been conducted at Mach 2.5, to determine the nature of flow controlled by micro-ramps and investigate their ability to delay separation in a reflected shock interaction. Various ramp sizes between 30% and 90% of boundary layer thickness were investigated. The details of the vortical flow generated by such devices was identified. The general flow features were found to scale with device height and it is suggested that smaller devices need to be placed closer to the expected adverse pressure gradients. When applied to a separated oblique shock SBLI micro-ramps were not observed to eliminate flow separation, although they were shown to break up separated regions. Other performance indicators across the SBLI were also improved through the application of the devices.

15. SUBJECT TERMS

16. SECURITY CLASSIFICATION OF:			17. LIMITATION OF ABSTRACT	18. NUMBER OF PAGES	19a. NAME OF RESPONSIBLE PERSON
a. REPORT	b. ABSTRACT	c. THIS PAGE			HOLGER BABINSKY
					19b. TELEPHONE NUMBER (include area code) +44 1223 339721

Understanding micro-ramp control of supersonic shock wave boundary layer interactions

Final report

Grant No.: FA9550-06-1-0387, 1 June 2006 – 31 May 2007

H. Babinsky

Cambridge University
Department of Engineering

Abstract: This project investigated the potential of micro-ramp sub-boundary layer vortex generators for control of oblique shock boundary layer interactions (SBLIs) which is relevant to supersonic engine inlets. These novel devices can delay shock-induced separation and improve boundary layer health, thus offering the potential to reduce the bleed requirement in intakes. Experiments have been conducted at Mach 2.5, to determine the nature of flow controlled by micro-ramps and investigate their ability to delay separation in a reflected shock interaction. Various ramp sizes between 30% and 90% of boundary layer thickness were investigated. The details of the vortical flow generated by such devices was identified. The general flow features were found to scale with device height and it is suggested that smaller devices need to be placed closer to the expected adverse pressure gradients. When applied to a separated oblique shock SBLI micro-ramps were not able to completely eliminate flow separation, although they were shown to break up separated regions. Other performance indicators across the SBLI were also improved through the application of the devices.

Introduction

Supersonic intakes must provide a stable, uniform, low-loss, subsonic flow to the engine face at all flight conditions. Because of the excessive shock losses incurred by Pitot intakes, mixed compression intakes are desirable for Mach numbers greater than two (Figure 1). Oblique shock waves are an efficient form of compression; however they interact with the boundary layer forming on the intake walls. Shock induced separation can trigger large scale unsteadiness. The unsteady aspects of SBLIs in particular, can have potentially dangerous effects on intake structures. It is therefore beneficial to control the flow either before or during the interaction process. The target of

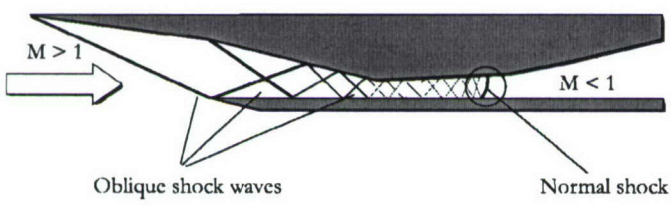

Figure 1. Mixed compression supersonic intake.

control is to prevent shock-induced separation and/or to stabilise the shock in naturally unsteady configurations.

Boundary layer bleed is the conventional form of flow control: low momentum fluid is removed through the porous intake surface. However, this reduces the engine mass flow rate below the capture mass flow rate, incurring a drag penalty. Reducing or eliminating bleed and its complex ducting will allow the intake frontal area to be reduced, which will reduce drag. Eliminating bleed, whilst maintaining intake performance, can therefore greatly increase aircraft range.

Conventional vortex generators (VGs), of a height of the order of the boundary layer thickness, have been used for some time to provide flow control in supersonic applications (Pearcey, 1961). More recently, attention has been turned to smaller *sub-boundary layer* VGs (SBVGs) with a height of approximately 40% of the boundary layer thickness that extend beyond the viscous sub-layer (McCormick (1993), Holden and Babinsky (2001), Lin (2002) and Ashill *et al* (2005)). It has been observed that SBVGs can reduce the boundary layer shape factor, making it more robust and hence less susceptible to separation. The principal benefit of SBVGs compared to conventional VGs is their reduced drag. A further advantage is that the vortices of counter-rotating devices can remain in the boundary layer for a significant streamwise distance, whereas those of VGs will lift off the surface more quickly. A particularly attractive quality of micro-ramps compared with other SBVGs is their physical robustness: intake manufacturers are unwilling to use fragile vortex generators, such as micro-vanes, that may break away during service, causing engine damage upon ingestion. Interest in micro-ramps has been initiated by Anderson *et al* (2006), whose RANS calculations indicate that the flow control afforded by micro-ramps is comparable to that of boundary layer bleed systems.

Experimental Set-up and Measurement Accuracy

Experiments have been performed in a blow-down supersonic tunnel. All tests were conducted at a nominal free stream Mach number of 2.5 and a Reynolds number of 30 x 10^6 m^{-1}. The wind tunnel stagnation Temperature was around 290K and the stagnation pressure was set to 170kPa (the exact value is variable during a typical experiment). A compression ramp on the upper surface of the tunnel is lowered in order to generate an oblique shock wave. For all the experiments reported here, the wedge angle was set to 7 degrees. The set-up is shown schematically in Fig.2.

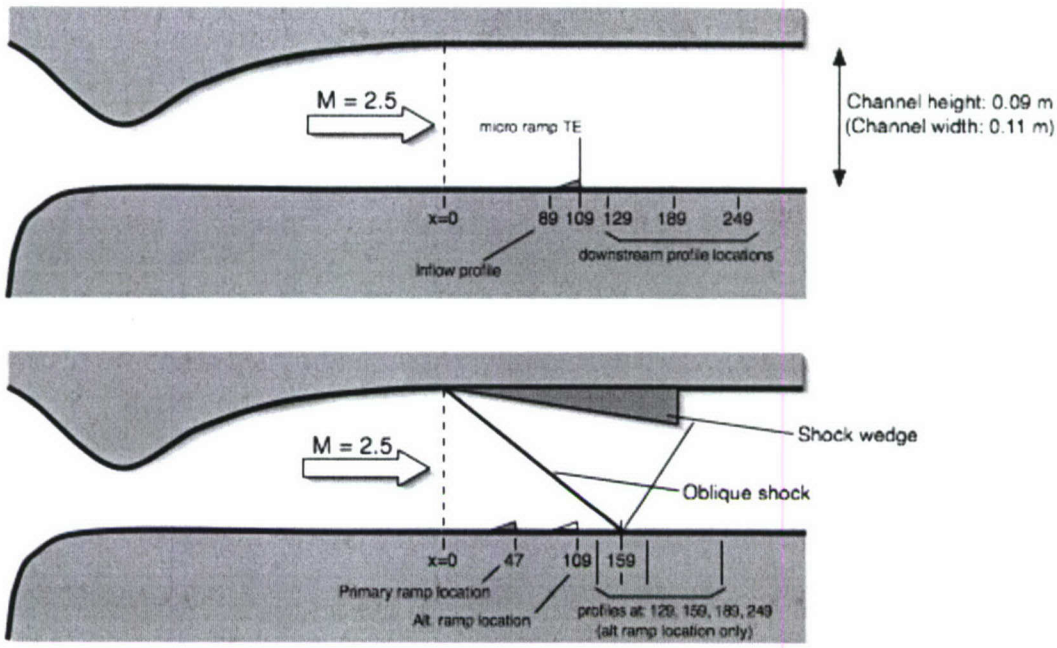

Figure 2. Experimental set-up for baseline experiments (top) and shock control experiments (bottom).

Geometrically similar micro-ramps of four sizes (heights 2 mm, 3 mm, 4 mm and 6 mm) have been tested. The micro-ramps are scaled according to the specifications of Anderson *et al* (2006) (Figure 3), so that the wedge half-angle α is equal to 24°, the side-length c is 7.2 times the device height h and the spanwise spacing s is 7.5 times h. Micro-ramps were investigated individually as well as in arrays. The number of micro-ramps in an array depended on their size: 6mm – 2 off; 4mm – 3 off; 3mm – 3 off; 2mm – 5 off.

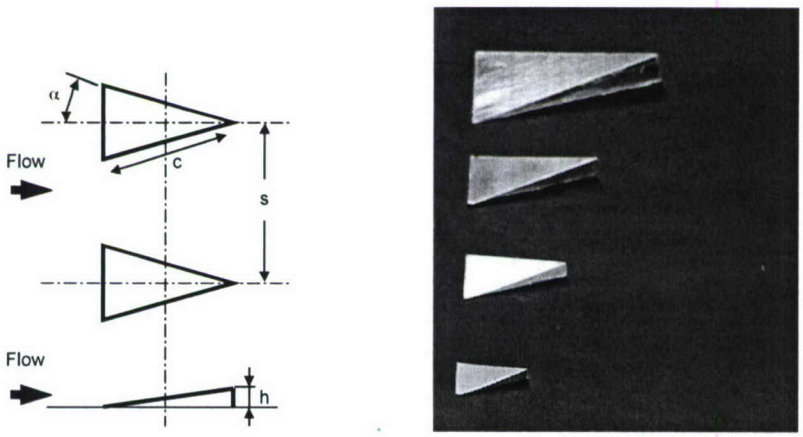

Figure 3. Micro-ramp geometry.

A combination of boundary layer traverses, schlieren photography, surface oil flow visualisation and surface pressure measurements are used to investigate the flow. Boundary layer traverses are conducted using a Pitot probe located at X=249mm which is moved through the boundary layer by a stepper motor. The upstream stagnation pressure and local static pressure are measured in addition to the pressure recorded by the Pitot probe. All pressures are recorded with fast-response Kulite transducers. Flow visualisation is carried out using a two-mirror schlieren system. The surface flow is visualised using a mixture of paraffin, titanium dioxide and oleic acid. Diesel oil is added to this mixture in order to prevent it drying before the flow was established. The surface pressure distribution is measured using pressure transducers linked to pressure tappings on the tunnel floor. The experimental uncertainty of surface and Pitot pressure measurements is of the order of ± 1%. The accuracy of the traverse gear is better than 0.5 mm. However, when using the Pitot data to determine boundary layer velocity profiles the effects of wall interference must be taken into account. Comparisons with LDA data have shown that Pitot data is subject to errors in a region up to 0.5mm from the surface. Consequently, integral properties determined from Pitot profile data has greater levels of uncertainty, of the order of 5-10%, although relative comparisons can be with more confidence.

One-component Laser Doppler Anemometry (LDA) was also employed to determine profiles of streamwise velocity at various stations (see Fig. 2). The DANTEC system in use featured a probe volume of 75μm diameter and approximately 2.5mm in length (aligned in spanwise direction). Seeding was obtained with oil droplets introduced in the settling chamber. The typical diameter of the seed particles was measured to be around 200nm. The combination of small probe volume and particle size allowed the determination of streamwise velocities down to a wall distance of 0.1mm. Typically, at least 1000 samples were used in the calculation of time-averaged velocities. The traverse gear used for the LDA investigation was of greater accuracy than that used for probe-based measurements, giving uncertainties of less than 0.05mm. Most of the LDA data was obtained along the centre-line. However, some profile measurements were recorded off-centre where the seeding density was lower. This has the effect of introducing noise into such LDA measurements (similar effects occur at large wall distances). When present, this is clearly seen in the data and spikes resulting from this effect can be ignored. The accuracy of LDA data obtained in regions of high seeding is very high, especially for the time-averaged velocities shown here. It is thought that velocities are determined to better than 1% accuracy (except for regions of poor seeding). For the purpose of comparison of this data with CFD predictions it should be noted that the total temperature during a typical experiment varied by approximately 5K. This introduces a corresponding variation of speed of sound which causes flow velocities to drift slightly during an experiment. While not exactly an experimental error, this nevertheless introduces an uncertainty in velocity data of the order of 5m/s in the free-stream.

Results

Flow development over micro-ramps (in the absence of shock waves)

Figure 4 shows the velocity profile determined with LDA in an empty working section (no shock generating wedge) at X=89mm. The boundary layer thickness is around 6mm and the (incompressible) integral values are: displacement thickness 0.96mm, momentum thickness 0.72mm and shape factor 1.32. The wall shear stress coefficient was estimated by fitting the velocity data to an analytical law-of-the-wall/wake profile suggested by Sun & Childs (1973), giving a value of 0.0015. These results are typical for a naturally grown, turbulent boundary layer in equilibrium.

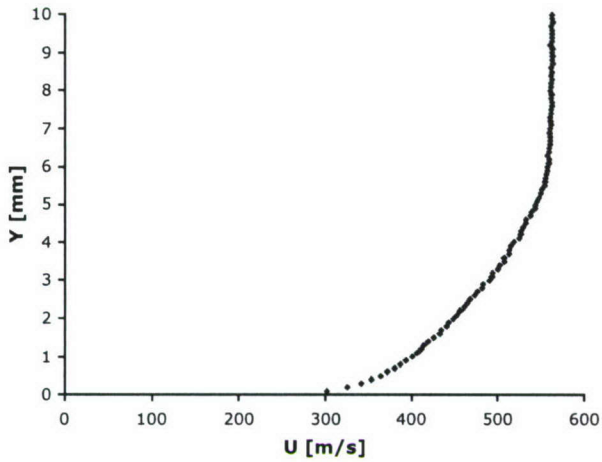

Figure 4. Inflow boundary layer profile (measured at x=89mm).

Figure 5 shows a schlieren image and surface oil-flow visualisation of the flow over a micro-ramp of 4mm height. In the schlieren photograph, the incoming boundary layer can be seen clearly and it is apparent that it is little affected by the presence of the device. Two shock waves originating at the leading and trailing edges of the ramp are also clearly seen. Less obvious is a faint edge downstream of the device which extends above the boundary layer. Later it will be shown that this is the upper edge of a vortical region.

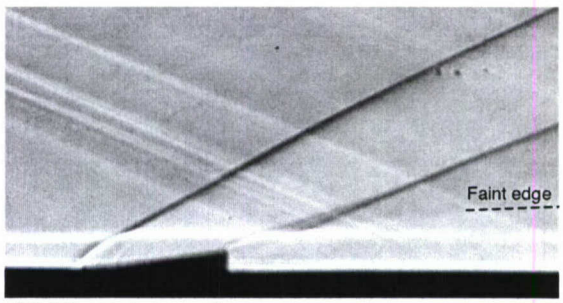

a) Schlieren photograph

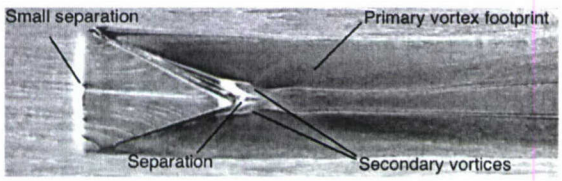

b) Surface Oil flow visualisation

Figure 5. Flow visualisation for 4mm height micro-ramp.

The surface oil-flow pattern suggests a region of comparably high shear in the wake of the micro-ramp, indicated by a darker colour. At the upstream edge of the device there is an indication of a small separation as the flow negotiates the compression ramp. This separation creates a very small horse-shoe vortex whose traces can also be seen either side of the high-shear wake. The main feature of the wake region is the herringbone footprint of two primary (counter-rotating) vortices. Another

feature is a small separation just after the downstream tip of the wedge. Also seen are secondary vortices originating from the side-wall/floor junction of the ramp and separated from the primary vortices by separation lines. Note that there are further secondary vortices originating from the top edge of the ramp, but these are not visible in the pictures shown. Close examination shows that the herring-bone pattern caused by the primary vortices fades some distance behind the ramp (of the order of 2 ramp lengths), suggesting that the vortices lift off the surface as a result of upwash induced by these vortices on each other.

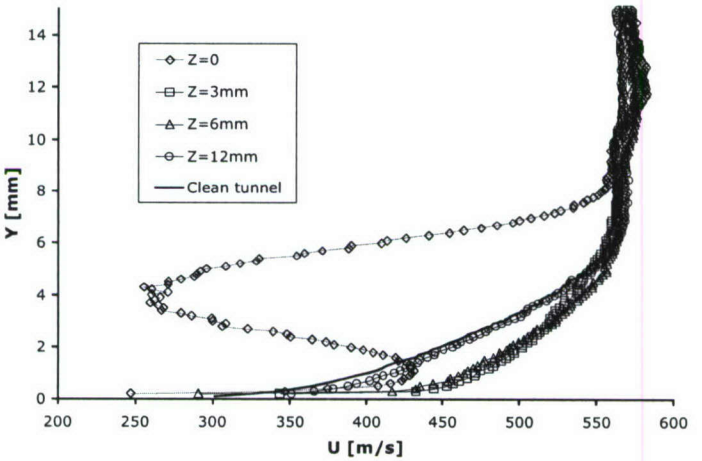

Figure 6. Velocity profiles at x=129mm (20mm downstream of ramp trailing edge) at various spanwise positions, 4mm height micro-ramp.

Figure 6 compares the velocity profiles measured downstream of a 4mm high micro-ramp at various spanwise locations (centre-line, quarter-chord, semi-chord and at full span). The furthest outboard profile (z=12mm) is very similar to the undisturbed boundary layer. This is in agreement with the oil-flow visualisation which indicated that the effect of the ramps did not reach far beyond the span of the device. Nevertheless, this profile and all others show increased velocities close to the surface, indicating high wall shear. Generally, the velocity profiles are fuller than the uncontrolled flow. However, the profile obtained at the centre-line features a pronounced low velocity 'dip' which is thought to be the remnant of the device wake that has moved slightly away from the surface as a result of the primary vortex action. The upper edge of this dip is responsible for the faint edge seen above the boundary layer in the schlieren photographs.

The main features of the boundary layer behind a micro-ramp become more clear when shown in the form presented in Fig.7. Here the velocities measured behind the device are subtracted from the undisturbed velocity profile. To generate the image a number of spanwise profiles have been used and symmetry has been assumed (the vertical bars at the top of the figure indicate where profile data was available). Because the data presented in Fig.7 has undergone significant processing this image should be used for illustrative purposes only (and it must be remembered that the spatial accuracy is limited by the small number of traverse positions). However, regions of high momentum near the surface and the low-momentum dip are seen very clearly. Even at this relatively small distance downstream of the ramps, there is already a considerable entrainment of high-energy flow near the floor which has almost covered all of the wake (except for a narrow region in the centre). The low momentum dip has begun to be moved away from the wall as a result of the action of the primary vortices.

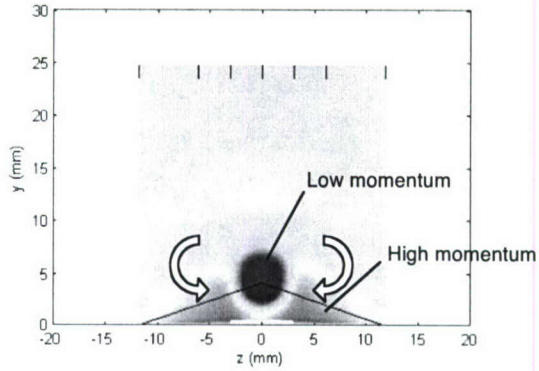

Figure 7. Streamwise momentum difference between ramp flow and baseline velocity profiles. The outline of the micro-ramp is indicated by thin lines for orientation.

The size of the micro-ramps has little effect on the fundamental flow features. This is illustrated by Figs. 8 & 9 which show the flows over the smallest and largest device tested (heights: 2mm & 6mm). The main flow features are almost identical to those seen above for the 4mm device.

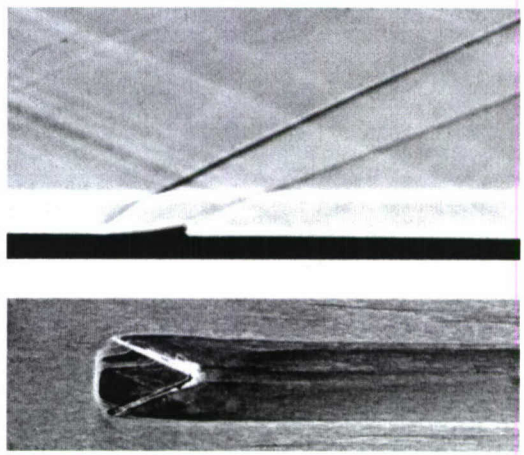

Figure 8. Schlieren photograph and surface oil flow visualisation for flow over 2mm micro-ramp.

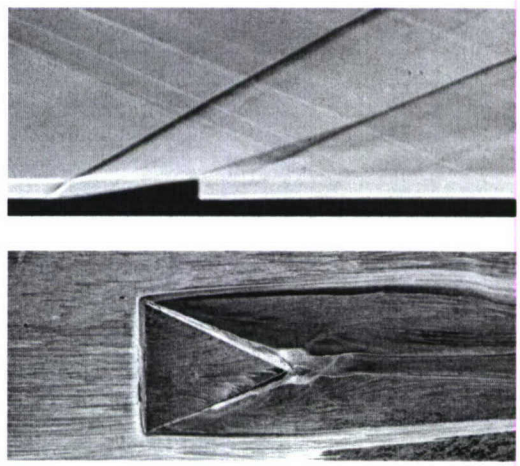

Figure 9. Schlieren photograph and surface oil flow visualisation for flow over 6mm micro-ramp.

A more detailed comparison of the effect of device height is shown in Fig.10. This shows the momentum difference at three streamwise stations downstream of each device for all device sizes examined. The exact locations of each traverse are as indicated in Fig. 2(top).

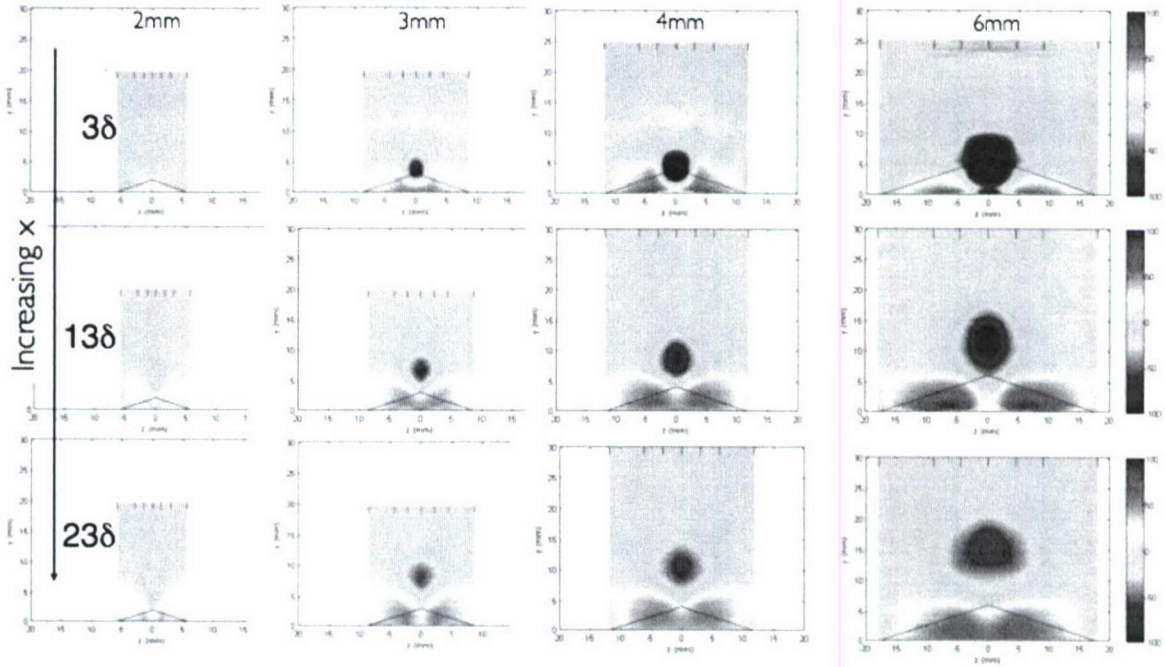

Figure 10. Streamwise momentum difference at various downstream locations for all devices tested.

The data shown in Fig.10 demonstrates that the flow development downstream of micro-ramps is similar for all device heights. In each case the low momentum wake (shown in blue) is gradually moved away from the wall by the action of the two primary vortices. Simultaneously, high momentum is entrained to the near wall region by the same mechanism. Closer inspection of this figure, however, suggests that the speed with which these processes occur is not the same across the devices. For example, in the first downstream profile (3δ) behind the largest device (6mm) there remains a considerable region of low momentum close to the surface around the symmetry plane. At the same downstream location behind the much smaller 3mm device however, the same area is already filled with high momentum fluid. This stage of development is only reached much later behind the largest device.

This suggests that the flow development, although similar for all sizes, does vary with device height. To test this hypothesis, the approximate height of the centre of the low momentum region (the blue area) is estimated from each of the sub-plots seen in Fig.10. The result is shown in Fig.11 in non-dimensional form; that is both the height above the surface as well as the streamwise distance from the device are divided by device height. It should be noted that the first data-point for the 2mm device is unlikely to be accurate as the low momentum region is too small to be accurately identified.

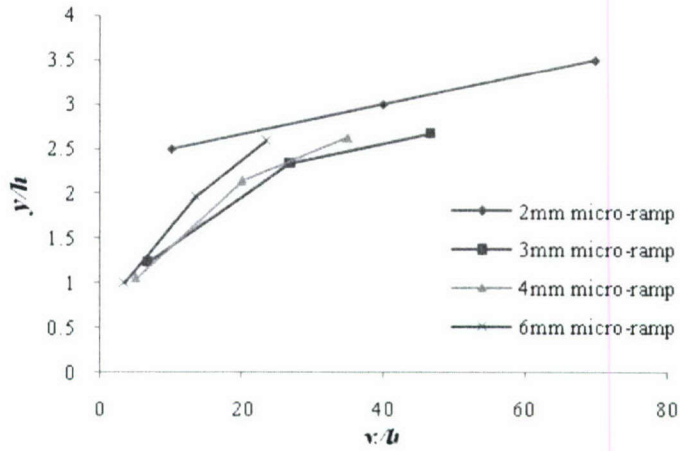

Figure 11. Non-dimensional height of low-momentum region (from Fig.10) as function of distance from device.

It can be seen that there is considerable agreement between the different curves which suggests that the flow development behind micro-devices may indeed scale with device height. A similar conclusion was reached by Ashill *et al* (2005) based on experiments performed on micro-VGs under incompressible conditions. The logical consequence of this would be that smaller devices generate vortices which are closer to the surface but lift off the wall more quickly than vortices generated by larger devices. In a practical application it would therefore be advisable to move smaller devices closer to the region requiring control.

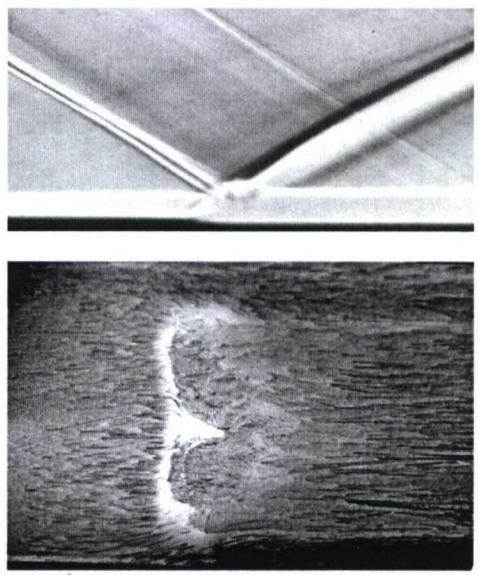

Figure 12. Schlieren photograph and surface oil flow visualisation for oblique shock reflection (7° wedge angle).

Effect of micro-ramps on reflected shock wave interactions

Figure 12 shows a schlieren photograph and surface oil-flow visualisation for the baseline uncontrolled interaction. It can be seen that the flow along the floor exhibits a relatively two-dimensional region of separation with a streamwise extent of approximately three incoming boundary layer thicknesses. Figure 13 compares the surface pressure measured along the tunnel centre-line for the baseline flow as well as a number of control configurations. Here, micro-ramps were placed 112mm ahead of the nominal shock reflection point (see Fig.2). Both individual devices (placed in the centre of the tunnel) as well as arrays of devices (spacing as shown in Fig.3) were tested. It can be seen that all devices reduced the upstream influence and increased the pressure gradient which is a sign of a reduction of separation. Clearly, arrays of devices performed better than single ramps and greater ramp heights proved slightly more effective.

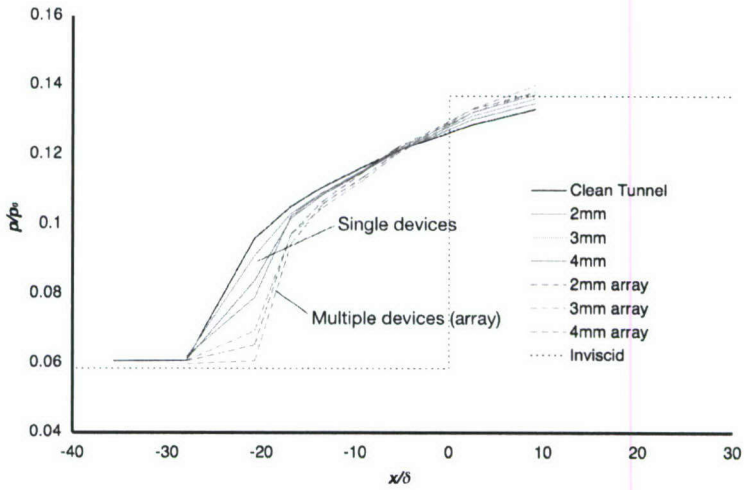

Figure 13. Centre-line surface pressure distribution through interaction with and without control.

Figure 14 shows typical surface oil-flow visualisations obtained for oblique shock reflections controlled by micro-ramps. It can be seen that the presence of micro-ramps causes a small region of attached flow in its immediate wake (approximately behind the device centre-line) and that the separated flow is broken up into a number of three-dimensional regions. When multiple devices are placed in an array, the number of cells increases in line with the number and placement of the ramps. While the presence of micro-ramps can not eliminate separation completely, it is seen to reduce the overall size of the separated region which is in line with the observations from the pressure measurements.

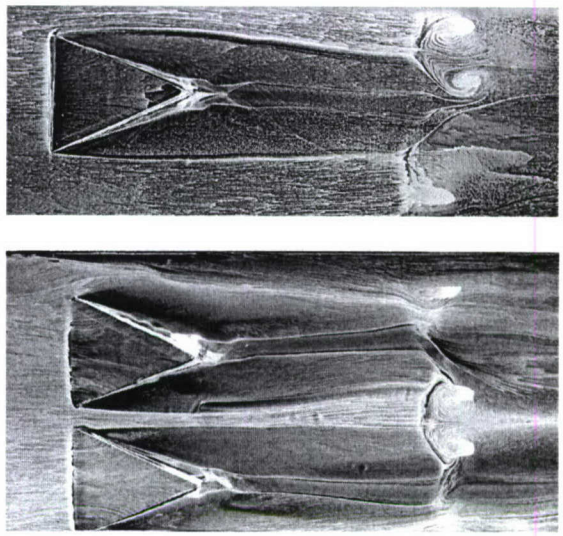

Figure 14. Surface oil-flow visualization for oblique SBLI controlled by single 6mm micro-ramp (top) and array of two 6mm micro-ramps (bottom). In both cases the separated region is broken up into a cellular structure.

The effect of streamwise placement relative to the interaction was also investigated. Figure 15 shows a schlieren photograph and surface oil-flow visualisation obtained for an array of 3mm micro-ramps placed closer to the location of interaction at a distance of 50mm (see also Fig.2). It can be seen that fundamentally the same flow structure as discussed above is observed.

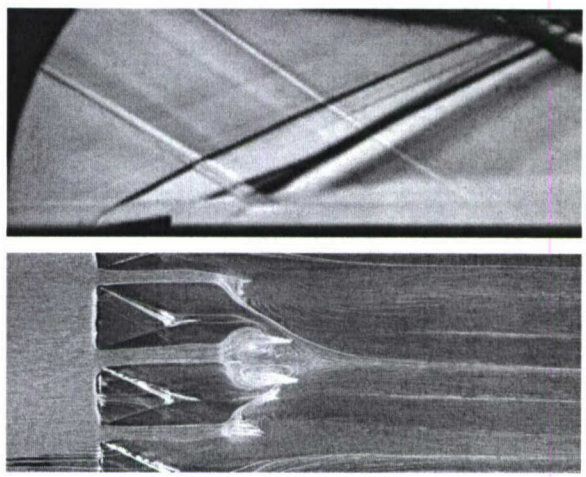

Figure 15. Schlieren photograph and surface oil-flow visualization for an array of 3mm micro-ramps placed 50mm upstream of the nominal shock reflection location.

Figure 16 compares the centre-line surface pressures measured for two device locations. It can be seen that there is little difference in the effect on the interactions. This suggests that the optimum location is somewhere in between the two positions tested here, or that streamwise position is not a very sensitive parameter.

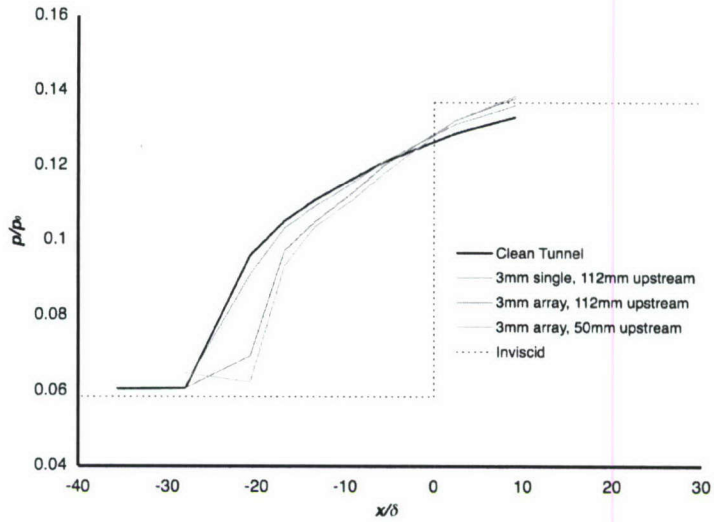

Figure 16. Centre-line surface pressure for interaction controlled with 3mm devices at two streamwise locations

Finally, Fig.17 shows velocity profiles measured across the interaction controlled by an array of 3mm devices located 50mm ahead of the inviscid shock reflection point (the configuration seen in Fig.15). Profiles were recorded at four streamwise positions (see Fig.2) ahead, through, and behind the interaction. For the interaction controlled by micro-ramps, profiles were also recorded at various spanwise locations relative to a device (centre-line, half-span and full span). It can be seen that all velocity profiles measured in the presence of the devices are notably fully near the surface. Velocity profiles recorded behind the centre of a device show evidence of the low momentum wake discussed earlier. This wake is seen to move away from the wall with downstream distance. Elsewhere, away from the centre-line of the device, the velocity profiles are significantly fuller and the boundary layer thickness has increased less through the interaction than in the uncontrolled case.

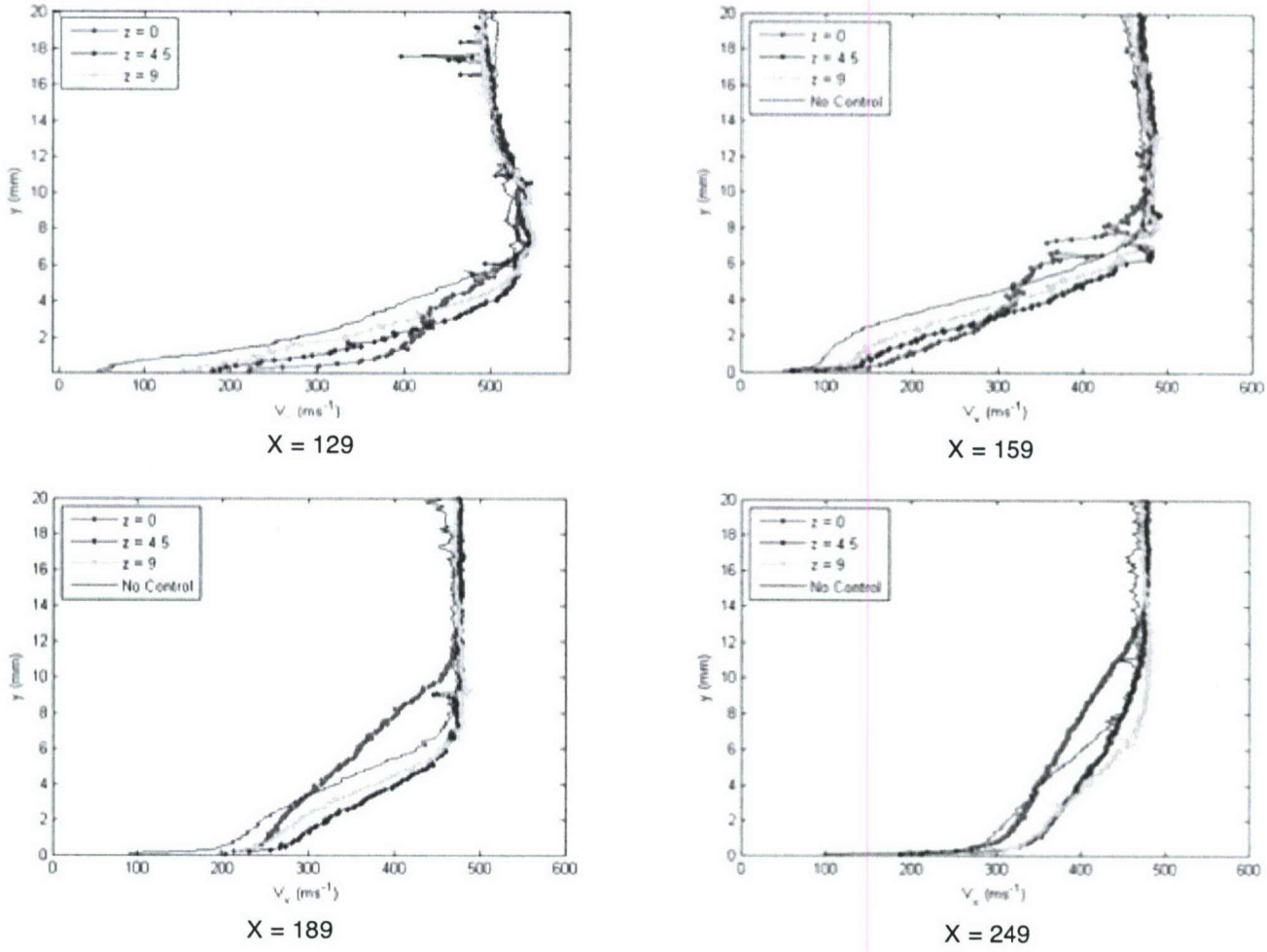

Figure 17. Streamwise velocity profiles measured with LDA at various streamwise and spanwise stations for the interaction controlled by an array of 3mm micro-ramps located 50mm upstream of the nominal shock reflection location.

For the more upstream location of control devices (see Fig.1) a complete survey of boundary layer profiles was recorded using a traditional Pitot tube at a streamwise location of X= 249mm (90mm downstream of the interaction). In each case integral boundary layer parameters were evaluated and the data is given in the appendix. This data, although less accurate than the LDA data shown above, also supports the main conclusions, namely that micro-ramp control reduces the boundary layer growth through the interaction and achieves fuller velocity profiles downstream. Larger ramps are seen to have the greatest effect, however this comes at a cost of increased device drag which is reflected in an increased momentum thickness. Smaller devices are seen to have beneficial effects without incurring a rise of momentum thickness. More detailed LDA measurements are required to fully evaluate the optimum device height and position, but this was not possible within the budgetary and time constraints of this project.

Conclusions

The flow over micro-ramps has been characterized with detailed measurements and flow visualizations. The information gathered is valuable for the understanding of micro-ramp flows as well as providing validation data for CFD simulations.

Downstream of micro-ramps a relatively complex structure of pairs of counter-rotating streamwise vortices is observed. Around the centre-line behind the ramp a significant low-momentum region is formed as a consequence of viscous drag of the device. The wake flow is dominated by the two primary vortices which act to entrain high momentum fluid from the outer regions of the boundary layer towards the surface. Simultaneously, the low momentum wake is transported away from the surface and has been observed to be deposited outside the boundary layer at some downstream distance from the device. The relatively complex vortical flow observed in the wake of micro-ramps can have subtle but important effects regarding the positioning of low and high momentum flow regions. The exact location of high and low momentum fluid is thought to be important for the devices' ability to prevent flow separation and it is therefore believed that numerical simulations need to be able to capture these effects correctly.

No fundamental change of the flow structure was observed with different micro-ramp sizes (heights from 30% - 100% of boundary layer thickness). However, it was suggested that the flow development can be scaled geometrically with device height.

Micro-ramps of all sizes were found to reduce separations in a M=2.5 oblique shock reflection, by breaking up a previously two-dimensional separation region into cells of separated flow (surrounded by attached flow). However, arrays of multiple devices distributed across the span had a much more beneficial effect than individual devices.

The largest ramp size tested was found to have the strongest effect, however it also incurred the greatest momentum deficit (ie drag). The smallest device height was able to have beneficial effects without incurring significant device drag.

No significant effects were observed when changing the device location relative to the shock reflection region, however, all locations tested were quite close to the interaction region. It is thought that micro-devices should be placed closer to adverse pressure gradients than traditional vortex generators and that the optimum location is likely to be a function of device height.

References

Anderson, B., Tinapple, J. & Surber, L. (2006) "Optimal Control of Shock Wave Turbulent Boundary Layer Interactions Using Micro-Array Actuation" AIAA Fluids Engineering Conference June, San Francisco.

Ashill P.R., Fulker J.L., Hackett K.C., (2005), "A Review of Recent Developments in Flow Control", *Aeronautical Journal*, Vol. 109, No. 1095, May 2005.

Holden H.A., Babinsky H., (2004) "Vortex Generators near Shock/Boundary Layer Interactions", 42nd AIAA Aerospace Sciences Meeting and Exhibit; Reno, NV; January 5-8, 2004

Lin J.C., (2002), "Review of Research on Low-Profile Vortex Generators to Control Boundary-Layer Separation", *Progress in Aerospace Sciences*, 2002.

McCormick D.C., (1993), "Shock/Boundary-Layer Interaction Control with Vortex Generators and Passive Cavity", *AIAA Journal*. Vol. 31, no. 1, pp. 91-96. January 1993.

Sun, C. C., and Childs, M. E., (1973), "A Modified Wall Wake Velocity Profile for Turbulent Compressible Boundary Layers," Journal of Aircraft, Vol. 10, 1973, pp. 381–383.

Publications resulting from this project

Pitt Ford, C.W., Babinsky, H., "Micro-Ramp Control for Oblique Shock Wave / Boundary Layer Interactions", AIAA 2007-4115

Further publication in preparation.

Appendix

Integral boundary layer parameters from Pitot pressure traverses performed downstream of micro-ramp controlled interaction. Micro-ramps were placed 112mm upstream of the inviscid shock reflection point and traverses were recorded at X=249 (90mm downstream of the inviscid shock reflection point). The spanwise location is given relative to the actual device. Position 1 is downstream of the ramp-centreline, position 3 is at the outer span and positions 2 and 4 are spaced as shown below to give uniform spanwise spacing. The actual positions differ with device size. Note that the accuracy of these Pitot data is limited. Typical errors are of the order of 5-10%. All parameters are calculated in their incompressible form (kinematic integrals only) and $\overline{H}_i$ is the arithmetic average of all four spanwise values.

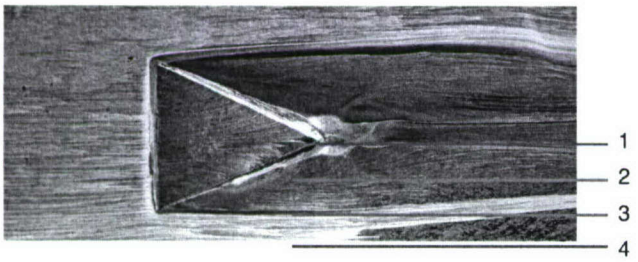

Micro-ramp	Location	δ^*_i / (mm)	θ_i / (mm)	H_i	$\overline{H}_i$
3 mm	1	2.03	1.61	1.26	1.30
	2	1.36	1.07	1.27	
	3	1.37	1.04	1.32	
	4	1.51	1.13	1.33	
4 mm	1	2.19	1.81	1.21	1.27
	2	1.27	1.03	1.23	
	3	1.29	0.98	1.32	
	4	1.36	1.02	1.32	
6 mm	1	2.65	2.27	1.17	1.25
	2	1.19	1.02	1.17	
	3	1.35	1.02	1.32	
	4	1.44	1.08	1.34	
No control	-	1.67	1.22	1.36	1.36